Received 13 June 2025; revised 17 August 2025; accepted 7 September 2025. Date of publication 16 September 2025; date of current version 26 September 2025.

Digital Object Identifier 10.1109/OJCOMS.2025.3610344

Quasi-Omnidirectional Vehicular VLC: Design, Implementation, and Experimental Validation

DANIEL K. TETTEY [1] (Student Member, IEEE), AND MURAT UYSAL [2,3] (Fellow, IEEE)

[1]Department of Electrical and Electronics Engineering, Özyeğin University, 34794 Istanbul, Türkiye
[2]Division of Engineering, New York University Abu Dhabi, Abu Dhabi, UAE
[3]Research Institute NYUAD Wireless Center, New York University Abu Dhabi, Abu Dhabi, UAE

CORRESPONDING AUTHOR: D. K. TETTEY (e-mail: daniel.tettey@ozu.edu.tr)

This work was supported in part by the Tamkeen under the Research Institute NYUAD under Grant CG017, and in part by the EU Horizon 2020 MSCA-ITN under Grant 814215 (ENLIGHT'EM).

ABSTRACT Visible Light Communication (VLC) is emerging as a compelling solution for future vehicular networks due to its high bandwidth and immunity to radio frequency (RF) interference. However, its relatively directional nature poses significant challenges in dynamic driving environments. This paper presents the first comprehensive experimental evaluation of a quasi-omnidirectional vehicular VLC system integrating dual headlight transmission with six photodetector (PD) receiver architecture. The system is implemented on a software-defined radio (SDR) platform and evaluated across a range of real-world driving scenarios including curved roads, intersections (T- and Y-junctions), and multilane settings. Through extensive outdoor measurements under static and mobile conditions, we demonstrate that our system achieves 100% packet delivery ratio (PDR) up to 15 meters in all scenarios and up to 29 meters under ideal alignment. We further compare select best combining (SBC) and equal gain combining (EGC) schemes, identifying SBC as the superior approach due to its noise robustness. Our findings show that strategically placed side and rear PDs play a critical role in maintaining connectivity during vehicular maneuvers, such as lane changes and turns. This study validates the feasibility and effectiveness of multi-PD vehicular VLC systems and provides key design insights for their integration into Intelligent Transportation Systems.

INDEX TERMS Connected vehicles, intelligent transportation systems, software-defined radio, USRP, visible light communication, V2X communication.

I. INTRODUCTION

THE SUCCESSFUL deployment of future intelligent transportation systems (ITS) will critically depend on robust wireless connectivity technologies capable of disseminating various sensor data between vehicles. This will enable the implementation of safety functionalities such as cruise control, parking assistance, and collision avoidance, as well as support infotainment applications. While earlier works [1] have mainly considered radio frequency (RF) bands for vehicular connectivity, the imminent spectrum crunch and the possibility of congestion in allocated bands under high dense vehicle scenarios prompt the need for alternative solutions.

Visible light communication (VLC) is based on the principle of modulating the intensity of light emitting diodes (LEDs) and was initially proposed for indoor use. The availability of LED exterior vehicle lighting, such as headlights and taillights, makes the use of VLC for vehicular connectivity possible [2], [3]. Unlike indoor deployments, atmospheric conditions and mobility must be taken into account in the design of vehicular VLC systems. To address the former, several channel characterization studies have been conducted [4], [5], [6], [7], [8], [9], [10], [11], [12], [13], [14], [15], [16]. Early works on vehicular VLC assumed simplified line-of-sight (LOS) channel models with Lambertian sources [4], [5], which are unsuitable for automotive headlights due to their asymmetrical intensity patterns. To address this, a piecewise Lambertian model was proposed in [6], while experimental measurements of headlamp distributions were presented in [7], [8], [9]. A closed-form path loss expression was later introduced in [10], though it is limited to clear weather and lacks explicit dependence on system parameters. The impact of weather conditions was further

© 2025 The Authors. This work is licensed under a Creative Commons Attribution 4.0 License.
For more information, see https://creativecommons.org/licenses/by/4.0/

TABLE 1. Experimental vehicular VLC works with more than one PD.

Ref.	No. Transmitters	No. Receivers	PHY layer	Environment	Measurement scenario
[12]	1 Tx	3 Rx	OOK	indoor	indoor lab measurement
[25]	1 Tx	2 Rx	OFDM	outdoor	outdoor static measurement
[27]	2 Tx	4 Rx	-	indoor	indoor lab measurement
[30]	1 Tx	2 Rx	OOK	outdoor	real-world vehicle test
[31], previous work	1 Tx	3 Rx	OOK	indoor	stationary vehicle test
This work	2 Tx	6 Rx	OOK	outdoor	comprehensive stationary and real-world vehicle test

explored in [11], [12], [13]. Most of these models are based on empirical fitting, limiting generalizability. The work in [17] overcomes this by deriving a closed-form path loss model based on non-sequential ray tracing, which accounts for headlamp asymmetry, weather-induced extinction, beam divergence, receiver aperture, and inter-vehicle geometry, offering a physically grounded, parameter-dependent framework to evaluate vehicle-to-vehicle (V2V) VLC performance across weather conditions.

The robust performance of vehicular VLC systems requires the use of multiple photodetectors (PDs) to ensure omnidirectional coverage in the presence of mobility. Most works in the literature assumed the deployment of one or two PDs placed at the back of the vehicle [6], [9], [13], [17], [18], [19], [20], [21], [22], [23], [24], [25]. This is typically sufficient to establish a connection between two vehicles cruising in the same straight lane with no or minimal horizontal displacement between them, such as in truck platoons. However, in urban driving conditions, vehicles frequently change lanes, turn at intersections, and exhibit larger lateral and angular displacements, making such limited PD configurations insufficient to maintain robust VLC links due to frequent blockages and misalignment. To ensure reliable reception on wider roads (e.g., two-lane) and curved roads, additional PDs are typically required. For example, in [26], three PDs are deployed and the one with the highest received power is selected as the primary receiver. In [27], the performance of the V2V system is investigated using an angle diversity receiver consisting of four PDs oriented in different directions. In [28], four PDs are used to prevent outages of a V2V system during lane change on a two-lane straight road. In [29], Eldeeb et al. presented a comprehensive ray tracing simulation study and argued that nine PDs with carefully determined locations on the vehicle are enough to create the required omnidirectional coverage for both V2V connectivity (in front and back directions) and infrastructure-to-vehicle (I2V) connectivity.

Experimental validation is essential to establish the feasibility, reliability, and practicality of vehicular VLC systems in real-world deployments. While the contributions in [28] and [29] offer valuable insights into the design of vehicular VLC systems, they lack experimental validation, which limits their applicability to real-world scenarios. As Table 1 illustrates, there is a limited number of experimental vehicular VLC studies that consider the use of more than one PD with a comprehensive outdoor measurement campaign.

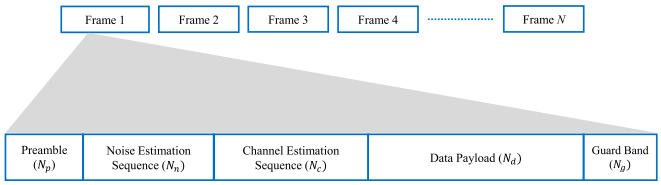


FIGURE 1. Transmission frame structure.

Particularly, in [30], Aly et al. experimentally evaluated a selection combining scheme for vehicular VLC system with two PDs placed at the side and back of a vehicle. The results in [30] demonstrate that selection combining improves link reliability by selecting the PD with the highest received signal strength. However, the utilization of a single headlight and two PDs cannot support V2V communication under more challenging road scenarios. Angle diversity receivers have been shown to create wide coverage in vehicular VLC. For example, in our previous work in [31], we experimentally investigated the use of an angle diversity receiver for vehicular VLC implemented with three PDs and showed that it can improve link reliability in curved road scenarios.

In this paper, we present the design, implementation and comprehensive experimental investigation of a vehicular VLC system across different road types, including straight roads, multilane roads, curved roads, and T- and Y-shaped intersections. For this purpose, we developed an experimental prototype using software-defined radio (SDR) platforms, providing flexibility in waveform generation and signal processing. The prototype is built upon USRP x310s with LabVIEW for signal processing. This setup enables system reconfigurability and real-time signal transmission and reception, allowing for extensive outdoor experimentation under real vehicular conditions. We investigated optimal signal combining techniques for the proposed multiple PD receiver architecture. We performed outdoor measurement campaign to evaluate the performance of the dual-headlight quasi-omnidirectional vehicular VLC system in various road scenarios, including straight roads, multilane roads, curved roads, Y-junctions, and T-junctions.

The rest of the paper is organized as follows: In Section II, we present the transmission signal models. In Section III, we describe the experimental setup and vehicular scenarios under consideration. We present the experimental results in Section IV. Finally, we present concluding remarks and future directions in Section V.

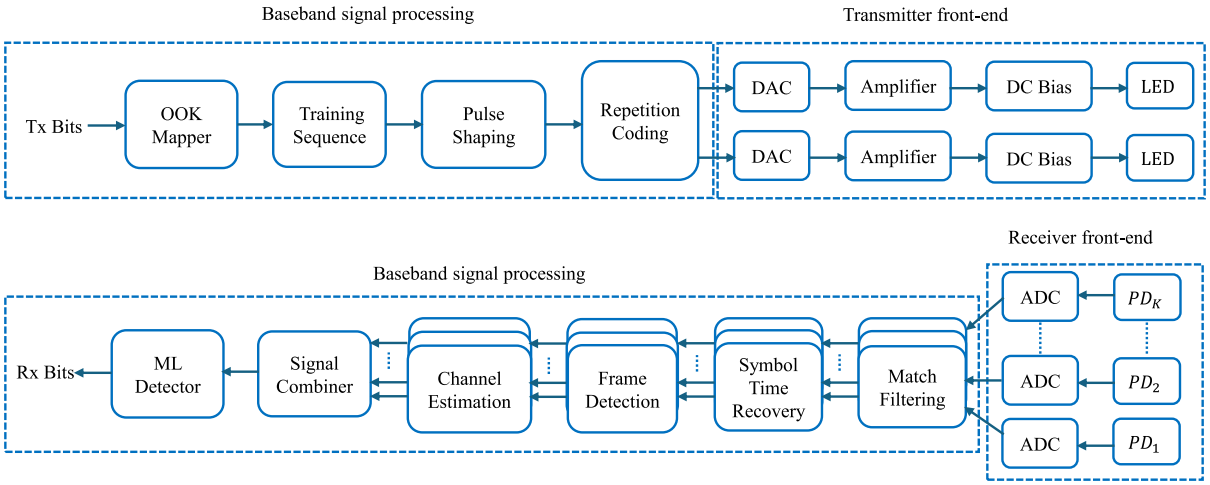


FIGURE 2. Block diagrams of transmitter (top) and receiver (down).

II. TRANSMISSION SIGNAL MODELS

We consider a unidirectional vehicular VLC system in which the headlights of the source vehicle are used to communicate with the destination vehicle. To improve communication reliability, we placed multiple PDs on the destination vehicle to ensure robust signal reception in various vehicular road scenarios.

As illustrated in Fig. 1, we consider a transmission frame of length L. Each frame begins with a preamble for frame detection, followed by a training sequence consisting of zeros and ones. After the training sequence, the data payload is to be transmitted is inserted. A short sequence of zeros is attached after the data payload to serve as a guard interval to mitigate inter-frame interference. The sequence of zeros is used for noise power estimation, whereas the sequence of ones is used for channel coefficient estimation. The frame structure has a preamble of length N_p, noise estimation training sequence of length N_n, channel training sequence of length N_c, data payload of length N_d, and a guard interval of length N_g.

The block diagrams of the transmitter and receiver are shown in Fig. 2. On the transmitter side, the message bits (Tx bits) are passed through an On-Off keying (OOK) symbol mapper. The transmit frame is constructed by multiplexing the payload with the preamble, channel and noise estimation sequences, and guard interval according to the frame structure presented in Fig. 1. The constructed frame is upsampled and filtered by a pulse-shaping filter. This is then passed through a repetition coding block to generate the same signal for the dual LED channels. The two outputs of the repetition coder are converted to analog signals using digital-to-analog converters (DAC). The analog signal from each DAC is amplified using an amplifier, and a direct current (DC) bias is added to the amplified signal to drive the LEDs.

Let $s(m)$ denote the m^{th} transmit symbol, where $m = 1, 2, 3, .., L$. We assume that both headlights are used to transmit the same message simultaneously. The electrical waveform driving each LED headlight takes the form of

$$w(t) = G\sqrt{\frac{P_t}{2}}\sum_{m=0}^{L-1} s(m)g_T(t - mT_s) + B_{dc}, \tag{1}$$

where, G denotes the amplifier gain, P_t is the average electrical transmit power, $g_T(t)$ is the impulse response of the pulse shaping filter, T_s is the symbol period, and B_{dc} is the DC bias. The DC bias is added to shift the message signal to the linear region of the LED headlight. A factor of 1/2 is multiplied by P_t to ensure that the total power consumed by both LED headlights is P_t. The transmit optical signal takes the form of

$$v(t) = \mu w(t) * l(t), \tag{2}$$

where, "$*$" is the convolution operator, μ is the electro-optical conversion ratio of the LED, and $l(t)$ is the impulse response of the LED headlight.

On the receiver side, there are K PDs placed around the destination vehicle to receive the optical signal from the source vehicle. Each of these PDs receives optical signals carrying the same message transmitted from the two LED headlights. The electrical output of the PDs is sampled by analog-to-digital converters (ADCs) for baseband processing. The sampled signals are convolved with a matched filter. After matched filtering, the received signal at the k^{th} PD, where $k = 1, 2, 3, .., K$, can be expressed as

$$r_k(t) = [Rv(t) * [h_{1k}(t) + h_{2k}(t)] + n_k(t)] * g_R(t), \tag{3}$$

where, R is responsivity of the PDs, and $g_R(t)$ is impulse response of the matched filter. Here, $n_k(t)$ is additive noise from the k^{th} PD modeled as white Gaussian noise.

In (3), $h_{1k}(t)$ and $h_{2k}(t)$ are optical channel impulse responses from left and right LED headlights respectively to the k^{th} PD. Substituting (1) into (2), (2) into (3), and simplifying the resulting expression yields (4), shown at the bottom of the next page, where $\widehat{B_{dc}} = R\mu B_{dc} * l(t) * [h_{1k}(t) + h_{2k}(t)] * g_R(t)$, $\widehat{n_k(t)} = n_k(t) * g_R(t)$. Here,

$\widehat{h_{1k}(t)} = \sqrt{P_t/2}R\mu G g_T(t) * l(t) * h_{1k}(t) * g_R(t)$ and $\widehat{h_{2k}(t)} = \sqrt{P_t/2}R\mu G g_T(t) * l(t) * h_{2k}(t) * g_R(t)$ denote the effective channel impulse responses that incorporate the overall effects of the transmitter and receiver front-ends, pulse-shaping filters, and the optical channel. Under the assumption that the effective symbol duration of the system is much longer than the duration of the channel impulse responses, we can approximate them as single tap channel coefficients, i.e., $\widehat{h_{1k}(t)} = \alpha_{1k}$ and $\widehat{h_{2k}(t)} = \alpha_{2k}$. Therefore, (4) is simplified as

$$r_k(t) = \alpha_k \sum_{m=0}^{L-1} s(m)\delta(t - mT_s) + \widehat{B_{dc}} + \widehat{n_k(t)} \tag{5}$$

where, $\alpha_k = \alpha_{1k} + \alpha_{2k}$ is defined as the effective superimposed channel coefficient.

After matched filtering, symbol time recovery is performed to locate the optimal sampling points of the received symbols using the maximum output energy method [32]. The symbols are sampled at the symbol rate of T_s. This is followed by a frame detection block, where a copy of the preamble is cross-correlated with the received frame samples to locate the beginning of the frame. The i^{th} sample of the data symbol (where $i = 1, 2, 3, \ldots, N_d$), at the k^{th} PD is given as,

$$r_k(i) = s(i)\alpha_k + \widehat{n_k(i)} \tag{6}$$

The individual PD output signals are combined in the form of

$$r(i) = \sum_{k=1}^{K} w_k r_k(i) \tag{7}$$

where, w_k is the associated signal combining weights for the k^{th} PD. The weights are selected according to the combining schemes, as will be discussed in the next paragraph. For both the detection process and the combining scheme, estimates of the effective channel gains are required. These gains are estimated as the average of the received channel training sequence, expressed as follows,

$$\widehat{\alpha_k} = \frac{1}{N_c} \sum_{j=0}^{N_c-1} r_c(j) \tag{8}$$

where, $r_c(j)$ is the received channel training sequence.

Two options are considered for the signal combining scheme. These are the select best combining (SBC) and equal gain combining (EGC). In the SBC scheme, the PD with the highest received signal strength is selected for symbol detection. Therefore, the index of the selected PD can be determined by

$$k_s = \arg\max_k \left(\frac{|\widehat{\alpha_k}|^2}{N_o} \right) \tag{9}$$

TABLE 2. System parameters.

Parameter	Symbol	Value
Average electrical transmit power	P_t	1 W
LED headlight's 3 dB bandwidth	BW	2.3 MHz
DC bias voltage	B_{dc}	26.5 V
Sample rate	F_s	2 MHz
Data payload length	N_d	1024 bits
Preamble length	N_p	64
Channel training sequence	N_c	100
Noise estimation sequence	N_n	100
Guard band length	N_g	50
Upsample factor	U	8
Data rate	D	250 kbps
RRC filter roll-off factor	ρ	0.3

where N_o is the noise power estimated using the portion of the frame with sequence of zeros. The weight of each PD for SBC scheme is given by

$$w_k = \begin{cases} 1, & k = k_s \\ 0, & \text{otherwise} \end{cases} \tag{10}$$

For EGC, the signal combiner applies equal weights to the signals from all PDs. Finally, the symbol decision is determined using maximum likelihood detector given as

$$\widehat{s}(i) = \min_l |r(i) - c(l)\widehat{\alpha_k}|^2 \tag{11}$$

where $c(l)$ represents the candidate symbols in the OOK constellation and $l = 1, 2$.

III. EXPERIMENTAL SETUP AND VEHICULAR SCENARIOS

A. EXPERIMENTAL SETUP

In this section, we describe the experimental design and implementation of the vehicular VLC system under consideration. Fig. 3 illustrates the experimental setup and the system parameters used in the experimental setup are summarized in Table 2.

The transmitter section as shown in Fig. 3(a) consists of an Ettus USRP x310 equipped with two low-frequency transmitter (LFTX) daughterboards. The USRP x310 is connected to a computer that runs the baseband signal processing algorithms as detailed in the previous section. All signal processing algorithms are implemented in LabVIEW. A square root-raised cosine (RRC) pulse-shaped transmit signal is generated according to the frame structure shown in Fig. 1. The frame has a preamble of length $N_p = 64$, noise estimation sequence of length, $N_n = 100$, channel training sequence of length $N_c = 100$, data payload of length $N_d = 1024$, and a guard band of length $N_g = 50$.

$$r_k(t) = \left[\sum_{m=0}^{L-1} s(m)\delta(t - mT_s) \right] * \left[\widehat{h_{1k}(t)} + \widehat{h_{2k}(t)} \right] + \widehat{B_{dc}} + \widehat{n_k(t)} \tag{4}$$

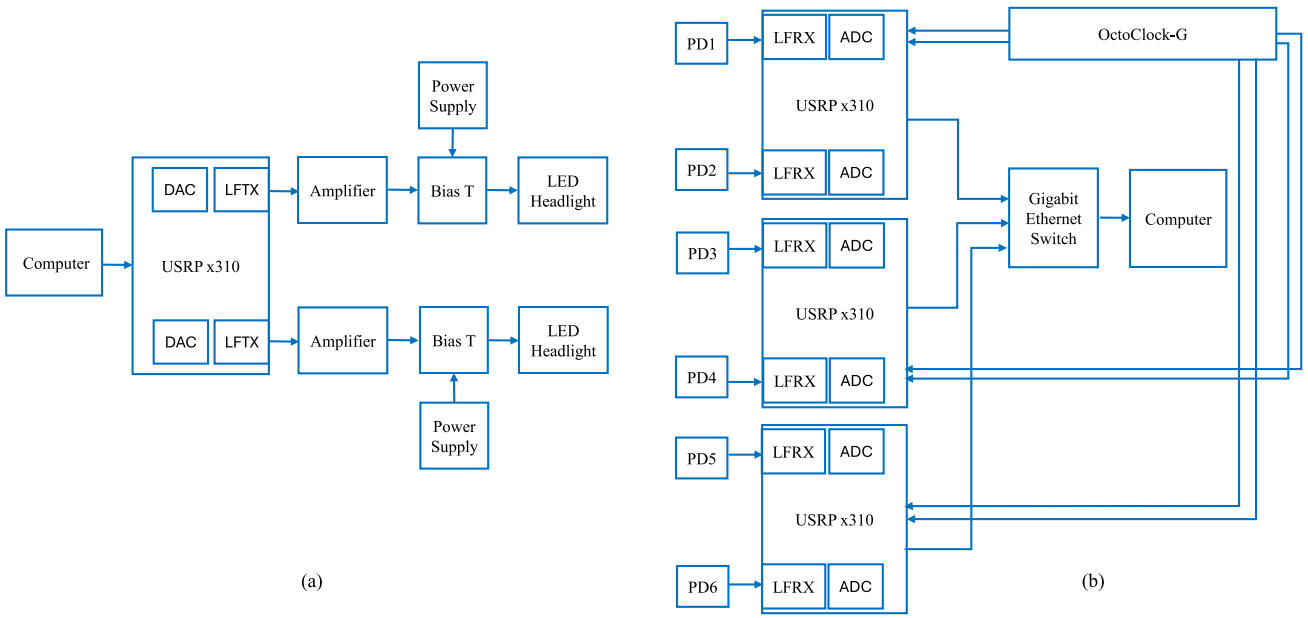


FIGURE 3. Experimental setup (a) Transmitter and (b) Receiver.

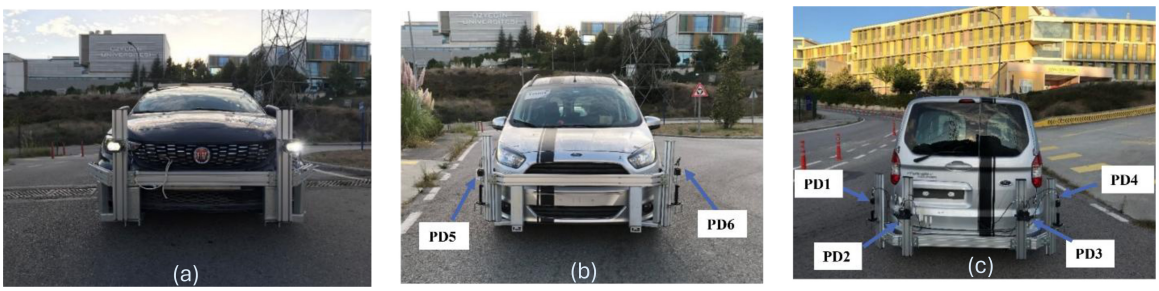


FIGURE 4. (a) Front view of source vehicle, (b) Front view of destination vehicle and (c) Rear view of destination vehicle.

At a symbol rate of 250,000 symbols/s and a frame length of 1338 symbols, the frame duration is approximately 5.35 milliseconds. Previous studies have shown that vehicular VLC channels vary slowly over time, with coherence times typically ranging from a few tens to several hundreds of milliseconds [20], [33]. Since the frame duration is much shorter than these values, the channel can be considered almost constant during transmission of a frame.

The pulse-shaped OOK transmit signal is converted to analog waveform by the USRP x310. The outputs of the USRP X310 are amplified using two Mini-Circuits ZHL-32A+ amplifiers, one for each channel. The amplified signal is then superimposed onto a 26.5 V DC bias using a custom-designed bias-tee. This high current bias-tee can support DC currents of up to 12 A with a 3 dB bandwidth of approximately 11 MHz [34]. The bias-tee ensures that the message signal remains within the linear region of the LED headlights to minimize clipping distortion. The output of the bias-tee is used to modulate the LED headlights. The LED headlights in the setup are the FORD F-MAX truck headlights, which have a 3 dB bandwidth of 2.3 MHz and a maximum output power of 26 W [34].

The receiver setup as illustrated in Fig. 3(b) consists of six Thorlabs PDA100A2 PDs connected to three units of Ettus USRP x310. Each USRP x310 is equipped with two low-frequency receiver (LFRX) daughterboards. To prevent saturation in the USRP, we used a Mini-Circuits DC blocker after each PD to filter out the DC component of the received signal. We used an OctoClock-G to provide a 10 MHz reference clock signal to synchronize the operation of all three USRPs. Optical signals received by the PDs are sampled by the USRP ADCs and forwarded to a computer via a gigabit Ethernet switch. The baseband receiver algorithms, implemented in LabVIEW, process the sampled signals according to the receiver block diagram illustrated in Fig. 2.

The source and destination vehicles used in our experiments are modified passenger vehicles. The modifications include fabrication and installation of metal frames around the source and destination vehicles to allow flexible attachment and removal of setup components. As shown in Fig. 4(a), the source vehicle features two LED headlights positioned at a height of 70 cm from the ground. The other components of the transmitter setup are housed inside the

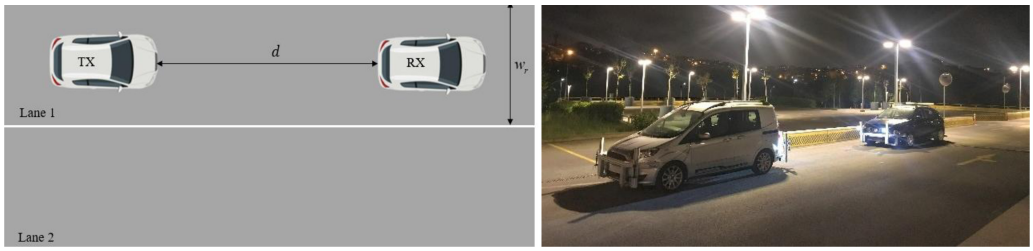


FIGURE 5. **Scenario 1** - Vehicles communicate with each other in perfect alignment ($d_h = 0$).

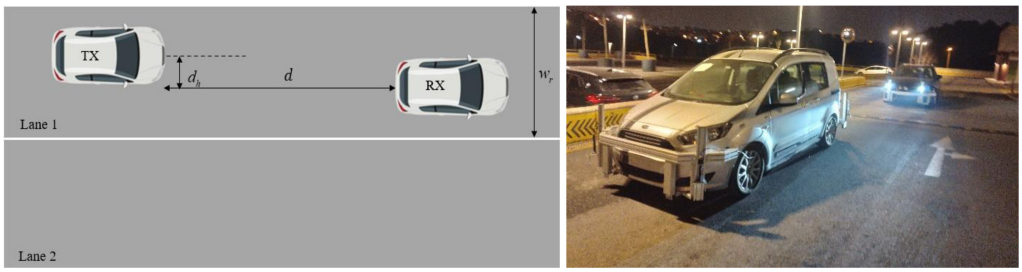


FIGURE 6. **Scenario 2** - Vehicles follow each other in same lane with small lateral shift ($d_h \neq 0$).

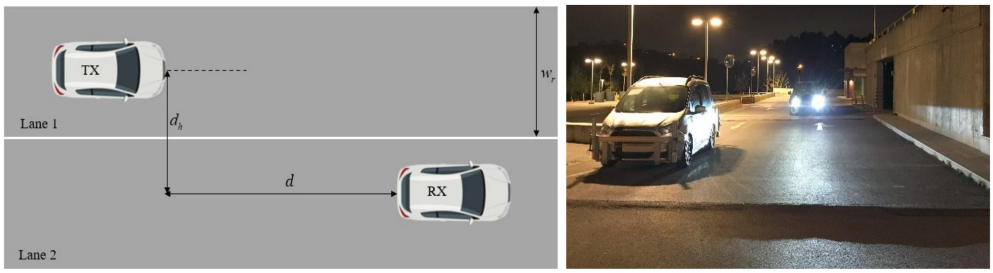


FIGURE 7. **Scenario 3** - Vehicles communicate with other in different lanes (wider lateral shift).

source vehicle. The destination vehicle, shown in Fig. 4(b) and 4(c), is equipped with six PDs, all mounted at a height of 65 cm from the ground. We denote the six PDs as PD1, PD2, PD3, PD4, PD5, and PD6. PD2 and PD3 are installed at the back of the vehicle. These two PDs are expected to be primarily useful to receive signals from the headlights. PD1 and PD4 are installed at the side-back of the vehicle using rotating optical stands. It is expected that PD1 and PD4 will be primarily useful when the source and destination vehicles are in different lanes or in a curved road. PD5 and PD6 are installed in front of the vehicle to receive signals from vehicles approaching in an adjacent lane. The USRP platforms are securely housed inside the source/destination vehicle and are powered by an uninterruptible power supply to ensure stable operation during the experiment.

B. VEHICULAR SCENARIOS

To evaluate the performance of our vehicular VLC system, we conducted an extensive measurement campaign on the university campus. We considered measurements in static and mobile conditions. The measurements under static conditions were carried out in the university car park, which features a two-way road with a lane width of 3.75 meters and a length of 55 meters.

First, we considered six static communication scenarios, as shown in Figs. 5–10. In **Scenario 1**, both vehicles are in the same lane without any misalignment. **Scenario 2** depicts the situation in which there is a lateral shift between both vehicles in the same lane. **Scenario 3** describes communication between two vehicles in different lanes but heading in the same direction. The communication of two vehicles at a T- and Y-junction (or curved road) are depicted in **Scenario 4** and **Scenario 5** respectively. Finally, **Scenario 6** illustrates a communication scenario on a two-way road with vehicles approaching each other in different lanes.

For each of the vehicular communication scenarios shown in Figs. 5–10, we transmitted 300 frames, each containing a data payload of 1,024 bits from the source vehicle to the destination vehicle at distance (d). For every frame received, performance metrics including received power, noise power, signal-to-noise ratio (SNR), bit error ratio (BER) and the selected PD used for receiving the frame are recorded. The experiment is repeated for different values of d until the end of the road. After taking measurements in static scenarios, we extended our experimental investigation with a real-world

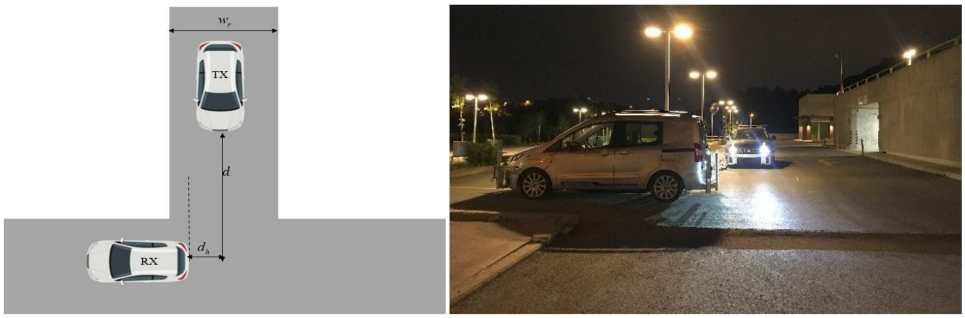


FIGURE 8. **Scenario 4** - Vehicles communicate with each other at a T-junction.



FIGURE 9. **Scenario 5** - Vehicles communicate with each other at a Y-junction.

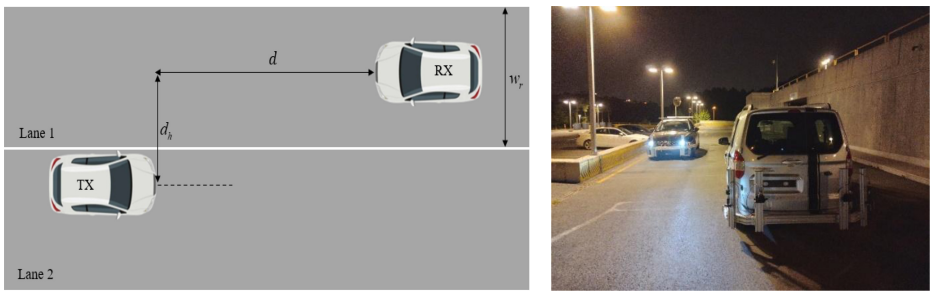


FIGURE 10. **Scenario 6** - Vehicles communicate while approaching each other in a two-way road.

driving test to evaluate the performance of the system in mobile conditions. Fig. 11 shows maps of two road tracks located on Özyeğin university campus where the driving tests are conducted.

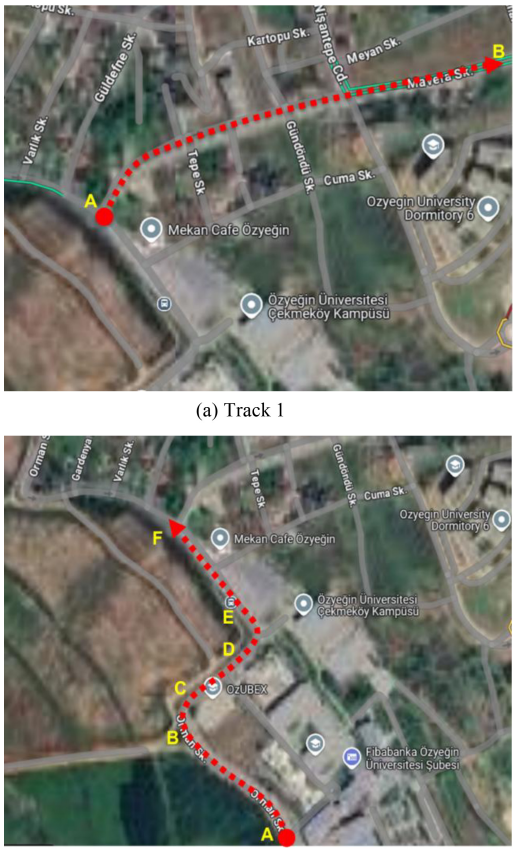
IV. EXPERIMENTAL RESULTS

A. PERFORMANCE COMPARISON OF COMBINING SCHEMES

To minimize the effect of ambient light on the measurements, static experiments covering different road scenarios were conducted at night between 8:00 and 10:00 pm. These tests focused on evaluating the fundamental behavior of the quasi-omnidirectional vehicular VLC system without strong external interference. In addition, vehicle driving experiments were carried out in the early morning hours (8:30-10:00 am) when sunlight intensity was moderate, to capture system behavior in daylight conditions while avoiding PD saturation.[1]

We conducted initial experiments to gain insight into the performance of two signal combining schemes, i.e., EGC and SBC. In these experiments, we considered a communication scenario on a straight road with perfect alignment between both vehicles as the best case scenario (Scenario 1, Fig. 5) and communication at a T-junction as the worst case scenario (Scenario 4, Fig. 8). Fig. 12 shows the received power at all PDs for the best and worst case scenarios at V2V distances of 6 meters, 21 meters and 49 meters. It can be seen that PD1, PD2, PD3, and PD4 received significant signal power in the

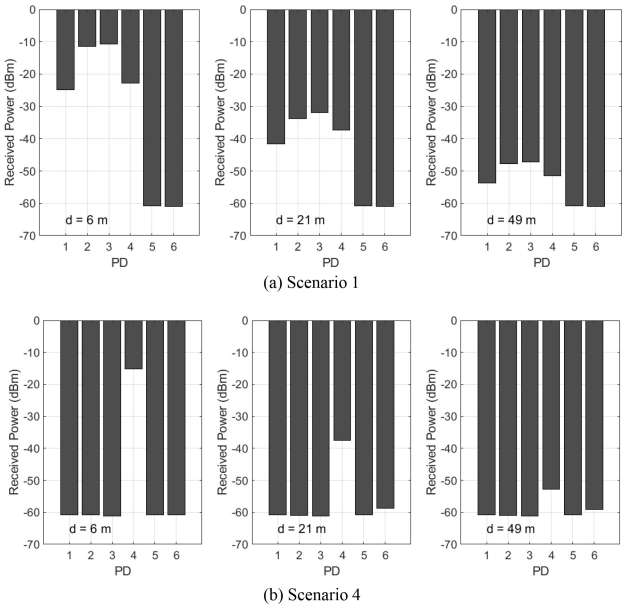
[1]To ensure reliable performance under strong sunlight, optical filters and automatic gain control (AGC) circuits can be employed, as discussed in [20].



(a) Track 1

(b) Track 2

FIGURE 11. (a) Track 1 - Road with straight lane (b) Track 2 - Road with straight lane and curves.



(a) Scenario 1

(b) Scenario 4

FIGURE 12. Received power for (a) Scenario 1, (b) Scenario 4, at $d = 6, 21,$ and 49 meters.

best case (Scenario 1), while only PD4 received significant power in the worst case (Scenario 4).

The received signal power and noise power at the output of the signal combiner for the best case (Scenario 1) and worst case (Scenario 4) are shown in Fig. 13. In Fig. 13(a), it can be observed that EGC outperforms SBC by at least 2.5 dBm in received power, as four PDs receive sufficient signal strength in the best case scenario (Scenario 1). However, SBC exhibits lower noise power compared to EGC, with a difference of about 8 dBm. This is because EGC fails to mitigate optical noise and interference due to the equal weights applied to signals from all PDs. As a result, its performance is degraded by the accumulation of noise from PDs receiving negligible optical signals. In Fig. 13(b), it can be observed that the received power for both SBC and EGC remains approximately equal across all distances considered. This is because, in such an extreme case of misalignment, only a single PD effectively receives the signal in both combining schemes.

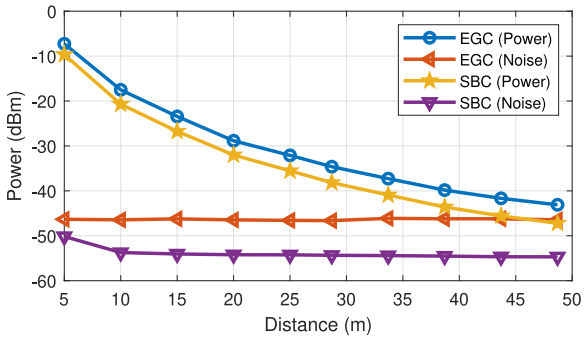
The comparison of the signal combiner outputs reveals that SBC consistently outperforms EGC in both the best (Scenario 1) and worst (Scenario 4) case scenarios. The performance gap arises because EGC combines signals from multiple PDs, including those with negligible signal contributions, which in turn introduces additional noise and reduces effective SNR. In contrast, SBC selects only the PD with the highest SNR, thereby avoiding noise-dominated signals and achieving more reliable performance. While EGC could in principle outperform SBC in perfectly aligned and static cases where several PDs receive equally strong signals, such conditions are uncommon in real V2V environments due to vehicle motion, lateral offsets, and dynamic road geometries. Consequently, SBC offers greater robustness across practical driving scenarios, which motivates its use as the signal combining strategy for the remainder of our experiments.

B. PERFORMANCE IN DIFFERENT VEHICULAR SCENARIOS

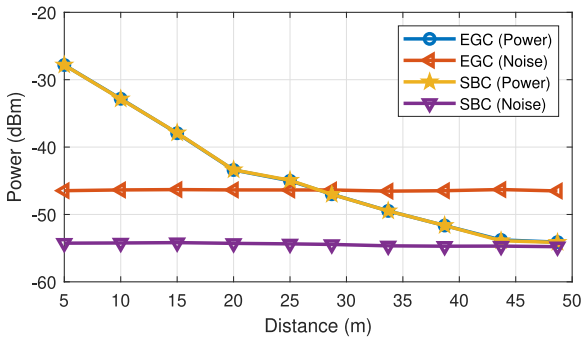
In this subsection, we present the measurement campaigns for scenarios 1 to 6, as illustrated in Figs. 5-10. In these measurements, the vehicles are not mobile. For each scenario, we performed several measurements at different distances, which can be considered snapshots of real-life driving conditions. We also discuss which PDs are selected in each case, providing insight into the robustness of vehicular VLC systems when multiple PDs are properly placed.

Fig. 14 shows the received power at each PD in Scenario 1 where the two vehicles are in perfect alignment. The experiment was performed at ten discrete distance values, selected within the transmission range of $d = 5$ meters to 49 meters. At $d = 5$ meters, PD2 and PD3 received the highest signal power (approximately -10 to -12 dBm), because they directly face the two headlights when both vehicles are aligned. Additionally, PD1 and PD4 received significant power due to their side-mounted positions at a 45° orientation angle.

In contrast, PD5 and PD6 recorded the lowest power levels (around –61 dBm) due to their placement at the front of



(a) Scenario 1: Received signal power and noise power



(b) Scenario 4: Received signal power and noise power

FIGURE 13. Received signal power and noise power vs. distance for (a) Scenario 1, (b) Scenario 4.

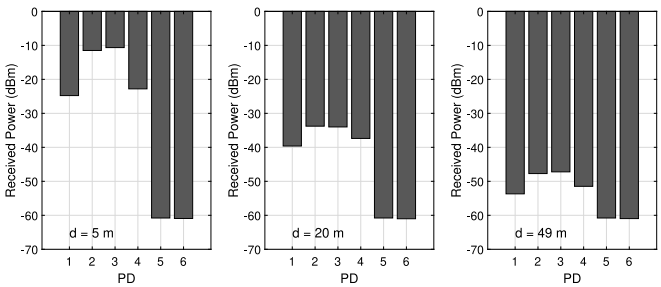


FIGURE 14. Received power levels in Scenario 1.

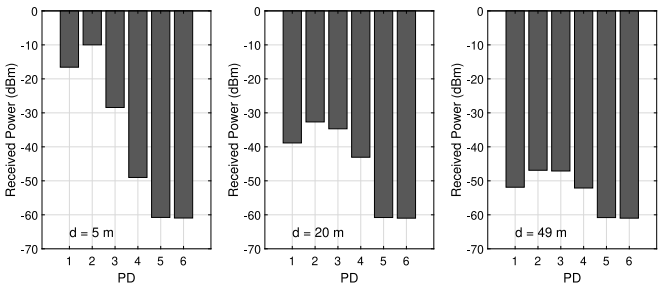


FIGURE 15. Received power levels in Scenario 2 ($d_h = 1.2$ meters).

the receiving vehicle. As distance increases, the received power decreases as shown in Fig. 14 for $d = 5$ meters, $d = 20$ meters, and $d = 49$ meters. For all measurements conducted at the ten different distances, PD3 was consistently selected as the primary PD due to its direct alignment with the headlight and marginally higher received signal strength than PD2.

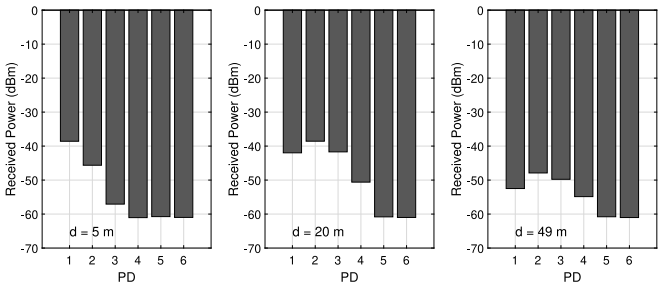


FIGURE 16. Received power levels in Scenario 3 ($d_h = 3$ meters).

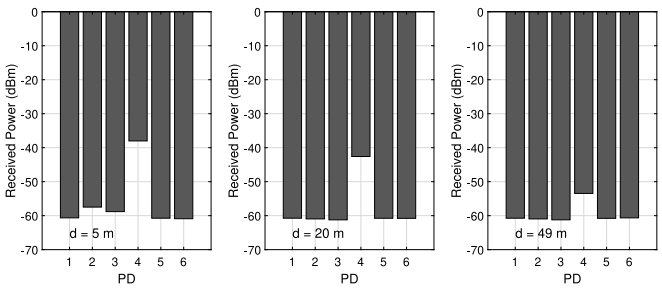


FIGURE 17. Received power levels in Scenario 4(b) ($d_h = 2$ meters).

Fig. 15 indicates the received power levels recorded for each PD in Scenario 2, where the vehicles are in the same lane and follow each other with a small lateral shift ($d_h =$ 1.2 meters). In this case, PD1, PD2, PD3, and PD4 received significant signal power, which gradually decreases as the distance increases.

Fig. 16 shows the received power of each PD in Scenario 3, where vehicles in different lanes communicate with each other. This effectively introduces a wider lateral shift (d_h = 3 meters) with respect to Scenario 2. Accordingly, the received power in this case is lower due to an increase in lateral shift from 1.2 meters to 3 meters. In this scenario, PD2 was selected as the primary detector at 80% of the ten distance points, whereas PD1 was selected at the remaining 20%. In Fig. 18, we show the received power levels of each PD in Scenario 4. Here, the vehicles communicate with each other at a T-junction with a lateral shift of d_h = 0.6 meters. In this scenario, PD4 received the highest power, as it was the only PD within the field of view of the vehicle headlights. Here, PD4 is selected as the primary PD and all other PDs recorded very low received power. These results highlight the role of side PDs in ensuring quasi-omnidirectional V2V coverage, particularly at curved road segments. Fig. 17 presents results for Scenario 4 but with an increased lateral shift of $d_h = 2$ meters. Compared to Fig. 18, the received power decreases with increasing lateral shift. For instance, at a lateral shift of $d_h = 0.6$ meters, the received power of PD4 at 5 meters is –15 dBm (see Fig. 18), whereas at $d_h = 2$ meters, it drops to –38 dBm as shown in Fig. 17. Similarly, PD4 acted as the primary PD for all the measurements at the ten varying distances. However, it is important to emphasize that if the lateral shift continues to increase, causing the primary PD to gradually vanish from

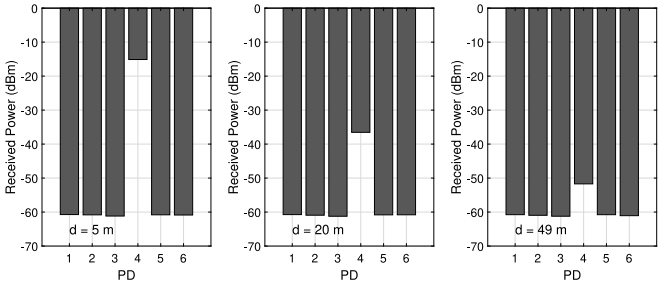


FIGURE 18. Received power levels in Scenario 4(a) ($d_h = 0.6$ meters).

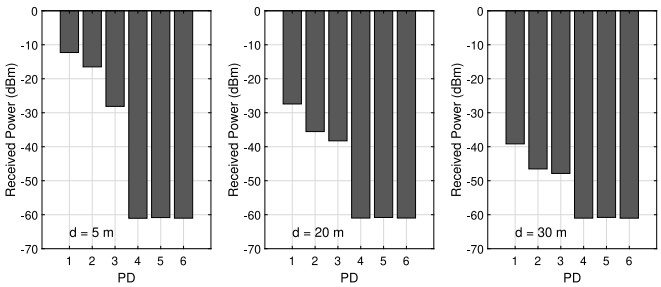


FIGURE 19. Received power levels in Scenario 5 ($\phi = 45°$).

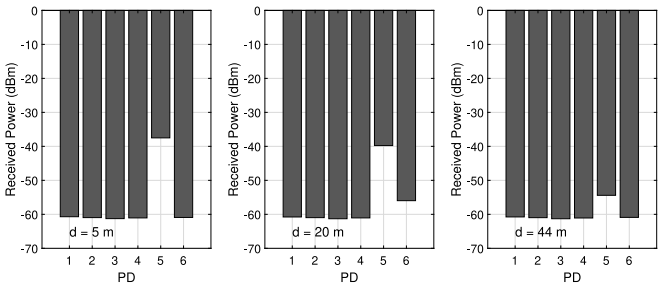


FIGURE 20. Received power levels in Scenario 6 ($d_h = 3$ meters).

the field of view of the headlights, the communication will eventually fail.

Fig. 19 shows the received power levels of each PD in Scenario 5. In this case, the vehicles communicate with each other at a Y-junction with an orientation angle of 45°. In this scenario, PD1, PD2, and PD3 are all within the field of view of the headlights, and therefore they received stronger signal than PD4, PD5, and PD6. PD1 was selected as the primary PD, as it received the strongest signal at all distances.

Fig. 20 shows the received power levels of each PD in Scenario 6 where the vehicles communicate while approaching each other on a two-way road. The lateral shift between the two vehicles is $d_h = 3$ meters. The received power of each PD at 5 meters, 20 meters, and 44 meters shows that PD5 received significant power of –38 dBm, –40 dBm, and –52.5 dBm, respectively. In this scenario, PD5 served as the primary detector. This highlights the importance of PD5 and PD6 in ensuring successful communication with vehicles approaching in adjacent lanes.

In Fig. 21, we present the measured SNR versus distance for different vehicular communication scenarios. The SNR is defined using (9) at the output of the SBC scheme. In

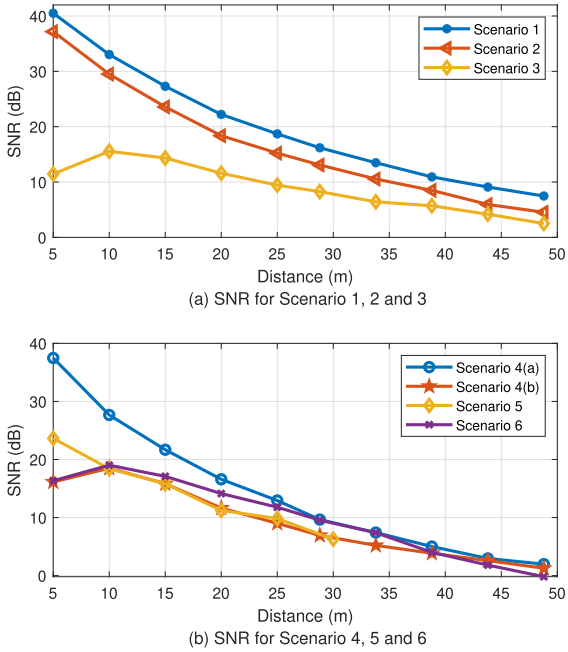


FIGURE 21. SNR for all vehicular scenarios in static conditions.

Fig. 21(a), Scenario 1 exhibits the highest SNR because the vehicles are strictly aligned. The SNR decreases in Scenario 2 due to a lateral shift of $d_h = 1.2$ meters between the vehicles. In Scenario 3, where the vehicles are in adjacent lanes and moving in the same direction with a lateral shift of $d_h = 3$ meters, the decrease in received power becomes more pronounced when compared to Scenarios 1 and 2. In Fig. 21(b), the SNR of Scenario 4 (with lateral shift of (a) $d_h = 0.6$ meters and (b) $d_h = 2$ meters) is compared to Scenarios 5 and 6. The SNR curve shows an exponential decline as the distance between vehicles increases.

Fig. 22 presents the packet delivery ratio (PDR), defined as the number of packets successfully transmitted to the destination vehicle without any bit errors. A total of 1,200 packets, each consisting of 1,024 bits, were transmitted at every distance. In Scenario 1, where the vehicles are perfectly aligned, a 100% PDR was maintained up to 28.8 meters. Beyond this distance, the PDR decreased from 100% to 89% at 33.8 meters due to decreasing signal strength as the distance increased. Notably, all communication scenarios including the worst-case scenario (Scenario 4) achieved a 100% PDR up to 15 meters.

C. PERFORMANCE IN MOBILE SCENARIOS

In the previous subsection, we carried out the experiments in static scenarios, which allowed us to make measurements in a controlled environment. In this subsection, we extend our experimental investigation by conducting a driving test to obtain performance measurements in mobile scenarios. The driving experiment took place in the morning between the hours of 8:00 am and 10:00 am since our experimental setup does not include noise mitigation techniques. During these

hours, the intensity of the Sun radiation was at moderate levels. The experiment was carried out on two different road tracks, as shown in Fig. 11. Track 1 features a straight road, while Track 2 shows a typical road with straight and curved segments. We drove the source and destination vehicles in a platoon-like scenario at an average speed of 20 km/h, keeping an average distance of 5 meters between the source and destination vehicles.

Fig. 23 presents the results obtained in Track 1. Fig. 23(a) shows the received power at each PD from point A to point B in Fig. 11(a). It can be seen that the PDs located at the back and sides of the destination vehicle (PD1, PD2, PD3, and PD4) received significant power. However, the front PDs (PD5 and PD6) received negligible signal power. Fig. 23(b) shows the received signal power and noise power at the output of the SBC scheme as we drove the vehicle from point A to point B. The system achieved a 100% PDR, as the received power did not experience any deep fades from point A to point B. Fig. 23(c) shows the PDs selected at the output of the SBC scheme from point A to B. Specifically, the rear PDs (PD2 and PD3) acted as the primary PDs during the drive test on Track 1. The selected PD alternated between PD2 and PD3 due to mobility induced lateral shifts between the source and destination vehicles. The percentage of PD selection is 71.56% for PD3, and 28.44% for PD2. An effective average SNR of 33.78 dB was achieved on Track 1, with a 100% PDR over the entire journey from point A to point B.

To evaluate the performance of our system on a more challenging road type, we performed another driving test on Track 2, from point A to point F as shown in Fig. 11(b). Due to the sharp curves, the orientation angles of the side mounted PDs, i.e., PD1 and PD4, whose main purpose is to support communication in curved road scenarios, were manually adjusted[2] to 62° and 47°, respectively. Fig. 24 presents the results of the driving test on Track 2. At the beginning of Track 2, the rear and back-side PDs received stronger signal. However, in the first curve (B to C), the rear PDs (PD2 and PD3) and PD1 experienced a sharp decrease in power (deep fade) due to the curved road segment. Meanwhile, the signal strength at PD4 increased and it became the primary PD along the curved segment of the Track until the next straight segment (C to D), where the rear PDs (PD2 and PD3) regained power. In the second curve segment (D to E), the rear PDs (PD2 and PD3) and PD4 experienced a deep fade due to their location. However, PD1 (a side PD) became the primary PD due to its location and manually adjusted orientation angle. In the curved segments, the primary PD switched to the side PDs,

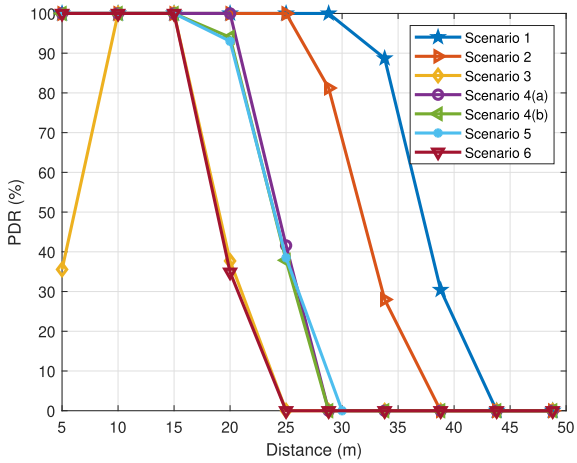


FIGURE 22. PDR vs distance for scenarios 1, 2, 3, 4, 5 and 6.

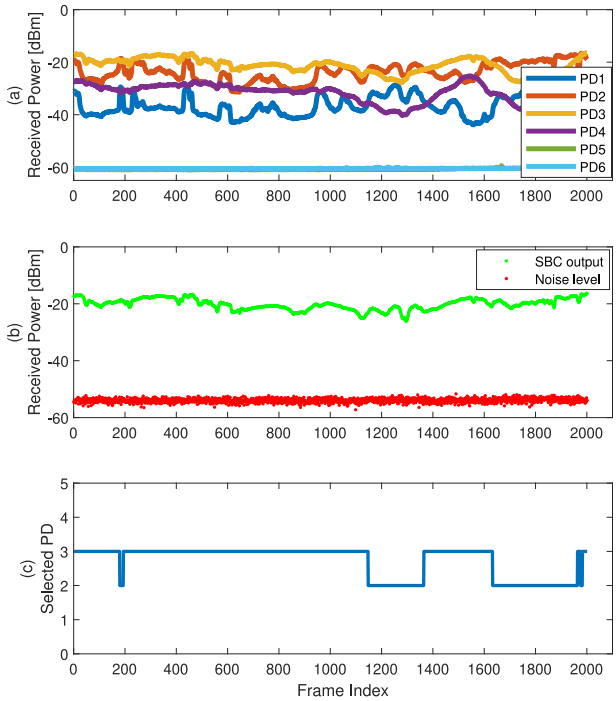


FIGURE 23. Measurement results in Track 1 (a) Received power at PDs (b) Received power at SBC output (c) Primary PD selection.

as they received the strongest signal. From point A to point F on Track 2, the percentage of PD selection during the drive test for PD1, PD2, PD3, and PD4 was 2.16%, 26.36%, 68.33%, and 3.15%, respectively. Although front PDs (PD5 and PD6) are beneficial in certain V2V scenarios, they proved less effective in this specific case. On average, our system achieved an SNR of 35.83 dB on Track 2, ensuring the successful delivery of 99.9% of the transmitted packets.

It is worth noting that during the experiments between points C and D on Track 2, PD4 occasionally faced direct sunlight and became saturated. However, since multiple PDs were available at the receiver, this saturation did not disrupt the communication link. This observation highlights another

[2]PD1 and PD4 were mounted on rotating optical stands, which allowed manual adjustment of their angles prior to the start of the mobility experiment. This approach is limited, as fixed angles may not guarantee a reliable communication link on different curved roads. In practice, a motorized, adaptively controlled, and electronically steered PD system would be more suitable and could be considered in future extensions of the experimental setup.

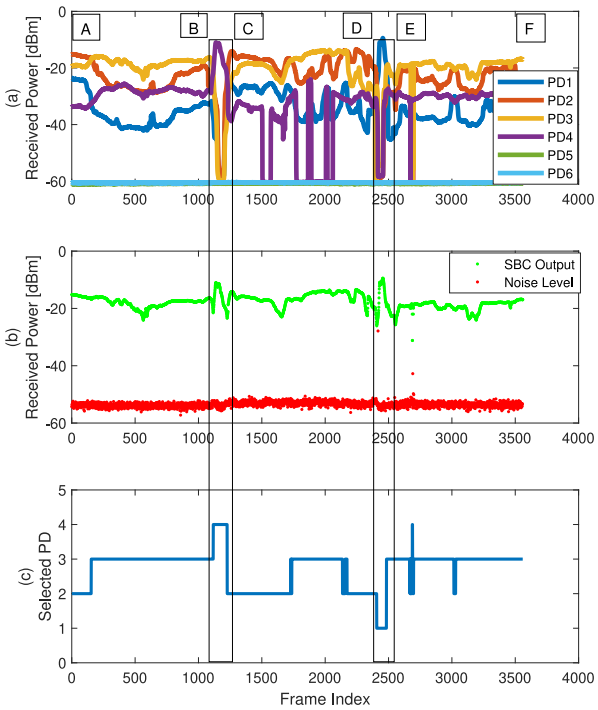


FIGURE 24. Measurement results in Track 2: (a) Received power at PDs (b) Received power at SBC output (c) Primary PD selection.

advantage of using multiple PDs, as it helps maintain link reliability in the presence of ambient light interference.

V. CONCLUSION AND FUTURE DIRECTION

In this paper, we have presented an experimental study on a quasi-omnidirectional vehicular VLC system, designed to improve V2V communication reliability in various road scenarios. Through an extensive measurement campaign under static and mobile conditions, the effectiveness of the system was validated in six different V2V communication scenarios, including straight roads, lateral shifts, T-junctions, Y-junctions, and two-way roads.

Our results demonstrate that the proposed system achieves a 100% PDR up to 15 meters, even under challenging misalignment conditions (T- and Y-junction). In a straight road with perfect alignment between vehicles, reliable error-free communication extends up to 29 meters. Furthermore, we extended the study to real-world driving experiments, validating the performance of the system under dynamic vehicular mobility. The results confirm that side-mounted PDs play a crucial role in maintaining communication at road curvatures, emphasizing the need for adaptive and reconfigurable PD orientation strategies to ensure omnidirectional vehicular VLC coverage in practical deployments.

It is important to note that this work considered a single transmitter–receiver vehicle pair, without interference from other vehicles. In real traffic environments, interference from surrounding headlights can reduce PDR. To address these challenges, future research should investigate robust interference mitigation strategies. Potential solutions include PD selection techniques, which leverage the angular sensitivity of optical receivers to reject unwanted light sources, and customized medium access control (MAC) protocols that regulate channel access to minimize collisions. Examples of such protocols include time division multiple access (TDMA), which schedules transmissions into non-overlapping time slots, and carrier sense multiple access with collision avoidance (CSMA/CA), which dynamically adapts transmissions based on channel sensing and contention resolution.

While our measurement campaign offers valuable insights into the system's performance under controlled conditions, it does not account for the effects of varying atmospheric phenomena such as fog, rain, or intense sunlight. These conditions can influence signal attenuation, scattering, and background noise levels, thereby impacting overall system reliability. A systematic investigation into the impact of such weather-related factors is another important direction for future work.

ACKNOWLEDGMENT

The authors acknowledge Mr. Mahir Huseyin Yesiller, Mr. Muhammet Emin Akbulut, and Dr. Mohammed Elamassie for their assistance with driving of the vehicles during the mobile experiment.

REFERENCES

[1] G. Karagiannis et al., "Vehicular networking: A survey and tutorial on requirements, architectures, challenges, standards and solutions," *IEEE Commun. Surveys Tuts.*, vol. 13, no. 4, pp. 584–616, 1st Quart., 2011.

[2] A. Memedi and F. Dressler, "Vehicular visible light communications: A survey," *IEEE Commun. Surveys Tuts.*, vol. 23, no. 1, pp. 161–181, 1st Quart., 2021.

[3] M. Uysal, Z. Ghassemlooy, A. Bekkali, A. Kadri, and H. Menouar, "Visible light communication for vehicular networking: Performance study of a V2V system using a measured headlamp beam pattern model," *IEEE Veh. Technol. Mag.*, vol. 10, no. 4, pp. 45–53, Dec. 2015.

[4] M. Akanegawa, Y. Tanaka, and M. Nakagawa, "Basic study on traffic information system using LED traffic lights," *IEEE Trans. Intell. Transp. Syst.*, vol. 2, no. 4, pp. 197–203, Dec. 2001.

[5] N. Kumar, D. Terra, N. Lourenco, L. N. Alves, and R. L. Aguiar, "Visible light communication for intelligent transportation in road safety applications," in *Proc. IEEE Int. Conf. Wireless Commun. Mobile Comput.*, 2011, pp. 1513–1518.

[6] W. Viriyasitavat, S. Yu, and H. Tsai, "Short paper: Channel model for visible light communications using off-the-shelf scooter taillight," in *Proc. IEEE Veh. Netw. Conf.*, Dec. 2013, pp. 170–173.

[7] S. J. Lee, J. K. Kwon, S. Y. Jung, and Y. H. Kwon, "Evaluation of visible light communication channel delay profiles for automotive applications," *EURASIP J. Wireless Commun. Netw.*, vol. 2012, pp. 1–8, Dec. 2012, Art. no. 370.

[8] P. Luo, Z. Ghassemlooy, H. L. Minh, E. Bentley, A. Burton, and X. Tang, "Fundamental analysis of a car-to-car visible light communication system," in *Proc. 9th Int. Symp. Commun. Syst. Netw. Digit. Signal Process.*, 2014, pp. 1011–1016.

[9] P. Luo, Z. Ghassemlooy, H. L. Minh, E. Bentley, A. Burton, and X. Tang, "Performance analysis of a car-to-car visible light communication system," *Appl. Opt.*, vol. 54, no. 7, pp. 1696–1706, Mar. 2015.

[10] A. Memedi, H. M. Tsai, and F. Dressler, "Impact of realistic light radiation pattern on vehicular visible light communication," in *Proc. IEEE Global Telecommun. Conf.*, Dec. 2017, pp. 1–6.

[11] Y. H. Kim, W. A. Cahyadi, and Y. H. Chung, "Experimental demonstration of LED-based vehicle to vehicle communication under atmospheric turbulence," in *Proc. IEEE Int. Conf. Inf. Commun. Technol. Converg.*, 2015, pp. 1143–1145.
[12] Y. H. Kim, W. A. Cahyadi, and Y. H. Chung, "Experimental demonstration of VLC-based vehicle-to-vehicle communications under fog conditions," *IEEE Photon. J.*, vol. 7, no. 6, pp. 1–9, Dec. 2015.
[13] M. Elamassie, M. Karbalayghareh, F. Miramirkhani, R. C. Kizilirmak, and M. Uysal, "Effect of fog and rain on the performance of vehicular visible light communications," in *Proc. IEEE 87th Veh. Technol. Conf.*, Jun. 2018, pp. 1–6.
[14] E. Eso, Z. Ghassemlooy, S. Zvanovec, J. Sathian, and A. Gholami, "Fundamental analysis of vehicular light communications and the mitigation of sunlight noise," *IEEE Trans. Veh. Technol.*, vol. 70, no. 6, pp. 5932–5943, Jun. 2021.
[15] P. Sharda and M. R. Bhatnagar, "Vehicular visible light communication system: Modeling and visualizing the critical outdoor propagation characteristics," *IEEE Trans. Veh. Technol.*, vol. 72, no. 11, pp. 14317–14329, Nov. 2023.
[16] P. Sharda, G. S. Reddy, M. R. Bhatnagar, and Z. Ghassemlooy, "A comprehensive modeling of vehicle-to-vehicle based VLC system under practical considerations, an investigation of performance, and diversity property," *IEEE Trans. Commun.*, vol. 70, no. 5, pp. 3320–3332, May 2022.
[17] M. Karbalayghareh, F. Miramirkhani, H. B. Eldeeb, R. C. Kizilirmak, S. M. Sait, and M. Uysal, "Channel modelling and performance limits of vehicular visible light communication systems," *IEEE Trans. Veh. Technol.*, vol. 69, no. 7, pp. 6891–6901, Jul. 2020.
[18] H. B. Eldeeb, E. Eso, M. Uysal, Z. Ghassemlooy, S. Zvanovec, and J. Sathian, "Vehicular visible light communications: The impact of taillight radiation pattern," in *Proc. IEEE Photon. Conf. (IPC)*, Sep. 2020, pp. 1–2.
[19] H. B. Eldeeb et al., "Vehicular VLC: A ray tracing study based on measured radiation patterns of commercial taillights," *IEEE Photon. Technol. Lett.*, vol. 33, no. 16, pp. 904–907, Aug. 2021.
[20] A.-L. Chen, H.-P. Wu, Y.-L. Wei, and H.-M. Tsai, "Time variation in vehicle-to-vehicle visible light communication channels," in *Proc. IEEE Veh. Netw. Conf. (VNC)*, Dec. 2016, pp. 1–8.
[21] B. Aly, M. Elamassie, H. B. Eldeeb, and M. Uysal, "Experimental investigation of lens combinations on the performance of vehicular VLC," in *Proc. 12th Int. Symp. Commun. Syst. Netw. Digit. Signal Process. (CSNDSP)*, Jul. 2020, pp. 1–5.
[22] A. Al-Kinani et al., "A 3-D non-stationary GBSM for vehicular visible light communication MISO channels," *IEEE Access*, vol. 8, pp. 140333–140347, 2020.
[23] A. Memedi, C. Tebruegge, J. Jahneke, and F. Dressler, "Impact of vehicle type and headlight characteristics on vehicular VLC performance," in *Proc. IEEE Veh. Netw. Conf. (VNC)*, Dec. 2018, pp. 1–8.
[24] H. B. Eldeeb, F. Miramirkhani, and M. Uysal, "A path loss model for vehicle-to-vehicle visible light communications," in *Proc. 15th Int. Conf. Telecommun. (ConTEL)*, Jul. 2019, pp. 1–5.
[25] Y. Wang, X. Huang, J. Shi, Y.-Q. Wang, and N. Chi, "Long-range high speed visible light communication system over 100-m outdoor transmission utilizing receiver diversity technology," *Opt. Eng.*, vol. 55, no. 5, May 2016, Art. no. 56104.
[26] Z. Cui, P. Yue, X. Yi, and J. Li, "Research on non-uniform dynamic vehicle-mounted VLC with receiver spatial and angular diversity," in *Proc. IEEE Int. Conf. Commun. (ICC)*, May 2019, pp. 1–7.
[27] M. Morales-Cespedes, A. A. Quidan, and A. G. Armada, "Experimental evaluation of the reconfigurable photodetector for blind interference alignment in visible light communications," in *Proc. 27th Eur. Signal Process. Conf. (EUSIPCO)*, Sep. 2019, pp. 1–5.
[28] H. B. Eldeeb and M. Uysal, "Vehicle-to-vehicle visible light communication: How to select receiver locations for optimal performance?" in *Proc. 11th Int. Conf. Electr. Electron. Eng. (ELECO)*, Nov. 2019, pp. 402–405.
[29] H. B. Eldeeb, S. M. Sait, and M. Uysal, "Visible light communication for connected vehicles: How to achieve omnidirectional coverage?" *IEEE Access*, vol. 9, pp. 103885–103905, 2021.
[30] B. Aly, M. Elamassie, and M. Uysal, "Vehicular VLC system with selection combining," *IEEE Trans. Veh. Technol.*, vol. 71, no. 11, pp. 12350–12355, Nov. 2022.
[31] D. K. Tettey, M. Elamassie, and M. Uysal, "Experimental investigation of angle diversity receiver for vehicular VLC," in *Proc. 29th Annu. Int. Conf. Mobile Comput. Netw. (ACM MobiCom)*, Madrid, Spain, Oct. 2023, pp. 1–8.
[32] R. W. Heath, *Introduction to Wireless Digital Communication: A Signal Processing Perspective*. Englewood Clifs, NJ, USA: Prentice-Hall, Mar. 2017
[33] Z. Cui, C. Wang, and H. Tsai, "Characterizing channel fading in vehicular visible light communications with video data," in *Proc. IEEE Veh. Netw. Conf. (VNC)*, Dec. 2014, pp. 226–229.
[34] B. N. Ashfaq, D. K. Tettey, and M. Uysal, "FPGA-based implementation and experimental demonstration of a vehicular VLC system," in *Proc. IEEE Virtual Conf. Commun. (VCC)*, 2023, pp. 282–287.



DANIEL K. TETTEY (Student Member, IEEE) received the B.Sc. degree in telecommunication engineering from the Kwame Nkrumah University of Science and Technology, Ghana, and the M.Eng. degree in electronic engineering from Hanbat National University, South Korea. He is currently pursuing the Ph.D. degree in electrical and electronics engineering with Özyeğin University, Türkiye.

He was a Marie Curie Ph.D. Fellow under the H2020 ENLIGHT'EM project at FORD Otosan, Türkiye. He is also a member of the OKATEM Research Lab, Özyeğin University. His research interests focus on wireless and optical communication, with particular emphasis on system development and prototyping of next-generation wireless systems using software-defined radio and embedded systems techniques. He has developed multiple experimental RF/VLC prototypes and demonstrations, which can be viewed at: https://www.youtube.com/@myWirelessDemos/videos.



MURAT UYSAL (Fellow, IEEE) received the B.Sc. and M.Sc. degrees in electronics and communication engineering from Istanbul Technical University, Türkiye, in 1995 and 1998, respectively, and the Ph.D. degree in electrical engineering from Texas A&M University at College Station, College Station, USA, in 2001.

He began his academic career as an Assistant Professor with the University of Waterloo, Canada, in 2002, and was promoted to an Associate Professor with tenure in 2007. In 2011, he joined Özyeğin University, Türkiye, where he served with the Department Chair of Electrical and Electronics Engineering and the Founding Director of the Center of Excellence in Optical Wireless Communication Technologies. Since 2023, he has been a Professor of electrical engineering with New York University Abu Dhabi. From 2011 to 2015, he was the Chair of EU COST Action OPTICWISE, a high-profile consolidated European scientific platform which brought together more than 150 researchers in the research area of optical wireless communication. On these topics, he has authored some 400 journal and conference papers and received more than 23.000 citations with an H-index of 67. His research interests are in the broad area of communication theory with a particular emphasis on the physical-layer aspects of wireless communication systems in radio and optical frequency bands. His major distinctions include the NSERC Discovery Accelerator Award in 2008, the University of Waterloo Engineering Research Excellence Award in 2010, the Turkish Academy of Sciences Distinguished Young Scientist Award in 2011, the Özyeğin University Outstanding Researcher Award in 2014, the National Instruments Engineering Impact Award in 2017, the Elginkan Foundation Technology Award in 2018, the IEEE Communications Society Best Survey Paper Award in 2019, the IEEE Turkey Section Outstanding Service Award in 2021, the Mustafa Prize, and the Tubitak Science Award in 2023. He currently serves as an Area Editor for the IEEE TRANSACTIONS ON COMMUNICATIONS. In the past, he served as an Editor for the IEEE TRANSACTIONS ON COMMUNICATIONS, the IEEE TRANSACTIONS ON WIRELESS COMMUNICATIONS, the IEEE TRANSACTIONS ON VEHICULAR TECHNOLOGY, and IEEE COMMUNICATIONS LETTERS. He was involved in the organization of several IEEE conferences at various levels. In particular, he served as the Technical Program Committee Chair of major IEEE conferences, including WCNC 2014, PIMRC 2019, and VTC-Fall 2019. He is the Former Chair of IEEE TURKEY SECTION.